EXOSKELETONS

A versatile knee exoskeleton mitigates quadriceps fatigue in lifting, lowering, and carrying tasks

Nikhil V. Divekar*, Gray C. Thomas†, Avani R. Yerva, Hannah B. Frame, Robert D. Gregg*

The quadriceps are particularly susceptible to fatigue during repetitive lifting, lowering, and carrying (LLC), affecting worker performance, posture, and ultimately lower-back injury risk. Although robotic exoskeletons have been developed and optimized for specific use cases like lifting-lowering, their controllers lack the versatility or customizability to target critical muscles across many fatiguing tasks. Here, we present a task-adaptive knee exoskeleton controller that automatically modulates virtual springs, dampers, and gravity and inertia compensation to assist squatting, level walking, and ramp and stairs ascent/descent. Unlike end-to-end neural networks, the controller is composed of predictable, bounded components with interpretable parameters that are amenable to data-driven optimization for biomimetic assistance and subsequent application-specific tuning, for example, maximizing quadriceps assistance over multiterrain LLC. When deployed on a backdrivable knee exoskeleton, the assistance torques holistically reduced quadriceps effort across multiterrain LLC tasks (significantly except for level walking) in 10 human users without user-specific calibration. The exoskeleton also significantly improved fatigue-induced deficits in time-based performance and posture during repetitive lifting-lowering. Last, the system facilitated seamless task transitions and garnered a high effectiveness rating postfatigue over a multiterrain circuit. These findings indicate that this versatile control framework can target critical muscles across multiple tasks, specifically mitigating quadriceps fatigue and its deleterious effects.

INTRODUCTION

Fatigue is inevitable and detrimental in physically demanding jobs. According to the US National Safety Council, 69% of workers across the construction, manufacturing, transportation, and utility industries get fatigued, increasing the risk of injuries and incidents on the job (*1*). Fatigue causes a decrease in workers' cognitive and physical performance in their assigned tasks (*2*, *3*). This fatigue-induced performance decline becomes crucially deleterious (injurious) when a minimum performance level is imposed by factors outside the workers' control, such as lifting and placing objects on a conveyor belt (*4*). More than a million people in the United States suffered a nonfatal work-related musculoskeletal disorder in 2021 (*5*), most commonly lower back pain (*6*), and such injuries cost employers millions of dollars annually in worker compensation (*7*).

Repeated lifting-lowering (LL) activities are highly associated with overexertion and lower back pain (*8*). There are two common lifting techniques: stooping—lifting with the back and a flexed lumbar spine—and squatting—lifting with the legs while maintaining a neutral lumbar spine (*9*). Comparatively, stooping consumes less energy (*10*) and is associated with less perceived lower limb exertion and fatigue (*11*, *12*), whereas squatting is associated with less lumbar shear forces and lumbar passive tissue stress (*13*, *14*). The squat technique is favored by people who have previously incurred lower back injuries (*15*, *16*) because squatting prioritizes the safety of the ligaments and discs of the lumbar spine over the muscles of the lower limbs (*14*, *17*). Moreover, the national workplace labor guidelines (*18*), military manual lifting guidelines (*19*, *20*), and most physical therapists (*21*) recommend the squat technique to prevent lower back pain, especially for lifting weights placed between the feet. Overall, squatting is often considered safer but is more energetically demanding and fatiguing on the quadriceps (*22*).

University of Michigan, Ann Arbor, MI, USA.
*Corresponding author. Email: ndivekar@umich.edu (N.V.D.); rdgregg@umich.edu (R.D.G.)
†Present address: Texas A&M University, College Station, TX, USA.

Quadriceps fatigue has been shown to influence a person's lifting technique, causing a transition from squatting to stooping as fatigue progresses (*23*). Consequently, high quadriceps fatigue is associated with higher effort of the lower back extensor muscles during repeated LL (*24*), increasing the chance of overuse injuries. The quadriceps are also critically involved in load-carrying tasks (*25*), including on ramps and stairs, which are frequently performed in many work environments (*18*, *26*–*29*). Although injuries are less common during carrying (*30*), these demanding activities further contribute to quadriceps fatigue (*31*) and subsequent injury risk during LL. Hence, solutions are needed to reduce contributions to quadriceps fatigue during lifting, lowering, and carrying (LLC) and to mitigate the deleterious effects of fatigue on LL, during which most injuries occur.

Although passive knee orthoses (exoskeletons) have been developed to support the quadriceps during LL (*32*, *33*), a fixed spring (even with a mechanical clutch) cannot adapt assistance over a variety of carrying tasks, especially those requiring net positive work. Similarly, passive hip-back devices can reduce lumbar moments during forward bending (*34*) but hinder hip flexion or lumbar flexion in walking (*35*). Newer commercial devices like the HeroWear Apex exosuit can be manually disengaged with a clutch when unrestricted lumbar flexion and/or hip flexion is desired (*36*), but the device then acts as a dead weight during multiterrain carrying tasks.

Robotic exoskeletons can adapt their assistance (including net changes in work) as the task changes (*37*, *38*), but existing designs for LL lack the versatility to support multiple carrying tasks. The robotic hip-back exoskeleton in (*39*) effectively supported LL but hindered walking. A subsequent study (*40*) overcame this limitation by classifying between LLC tasks, but the classifier was prone to errors and lacked multiple terrains. Moreover, these hip-back devices do not directly support the quadriceps muscles that are critically involved in both squatting and load-carrying. Using a combination of classification and human torque estimation, the hip-knee-ankle exoskeleton in (*41*) reduced activation of one quadriceps muscle during LL and the swing phase of walking but did not support

multiple terrains. A powered ankle exoskeleton reduced quadriceps activation by leveraging the closed-chain dynamics of squatting to induce helpful reaction torques at the knee (*42*–*44*). However, this dynamics phenomenon did not extend to the open-chain (single-support) phases of carrying. Although the commercial knee exoskeleton ROAM Forge can directly support the quadriceps during squatting tasks, it needs to be manually disabled for a dynamic gait because its pneumatic actuator impedes swing knee flexion (*45*). Although recent quasidirect drive actuators (*46*, *47*) are sufficiently backdrivable and torque dense to dynamically assist the knee, related devices have only reduced quadriceps effort and/or metabolic cost during LL (*48*, *49*). A versatile control strategy is needed for backdrivable knee exoskeletons to minimize quadriceps fatigue during multiterrain LLC and mitigate the consequences of fatigue during riskier LL tasks.

Although versatile controllers have been proposed for specific use cases, they lack the practicality, generality, or customizability for many applications like multiterrain LLC. One approach is to provide torques directly proportional to electromyography (EMG) measurements (*50*), but surface EMG electrodes are cumbersome to set up and are sensitive to positioning, sweat, and pressure from the exoskeleton. Another approach is to command torques proportional to biological torque, which generally aligns with muscle activation. For example, ankle torques can be directly estimated from the vertical ground reaction force (GRF) measured from an insole (*51*), but dynamic modeling errors and missing GRF components present substantial issues for more proximal joints. Alternatively, explicit representations of gait phase and task can parameterize a biomimetic torque model derived from human data. Machine learning methods are commonly used to classify discretized activity modes (*52*), but this does not allow adaptation to continuous variations in the environment or user behavior. Continuous adjustments in biomimetic ankle torque were achieved by estimating gait phase, ground incline, and walking speed in (*53*), but such phase models struggle with rapid transitions to and from stationary tasks like LL. Instead of explicitly representing tasks, emerging task-agnostic control approaches implicitly encode task-dependent input signals into an end-to-end mapping to biomimetic output torque. Recently, an end-to-end neural network trained from device-specific human data enabled a hip exoskeleton to predict and apply a fraction of human hip torques across multiple activities, reducing the users' metabolic cost for level walking (LW) and ramp ascent (RA) (*54*). Although valuable for some use cases, this global measure of effort is less pertinent when performance or posture is compromised by fatigue of a specific muscle group. This approach has also not been validated for the more variable kinetics of the knee, which change rapidly during certain task transitions such as walking to stair ascent. In general, "black box" learning methods lack formal safety guarantees for out-of-distribution input data and interpretable parameters for customization to different use cases or individuals [for example, via human-in-the-loop optimization (*42*, *55*)].

Our group has investigated another task-agnostic framework based on the nonlinear control method of energy shaping, which alters the dynamics (such as potential and inertial forces) of the human-exoskeleton system in a closed loop by applying joint torques as functions of the current system state (angles and velocities) (*56*, *57*). The solutions to partial differential equations called the "matching conditions" determine the realizable alterations to the dynamics of an underactuated system, which can be used to define a set of admissible torque basis functions that parameterize the controller. On the basis of the spring-loaded inverted pendulum walking model, our early work (*56*) used a minimal basis set (including gravity compensation and virtual springs and dampers) to provide assistive knee and ankle torques for incline, decline, and LW. Although intuitive and provably safe (via passivity/stability analysis), this controller could only handle limited walking tasks, and its assistance torque was not biomimetic. Our recent work (*57*) used human data to optimize the coefficients of a large set of torque bases to closely predict average torques given average kinematic inputs over the primary activities of daily life (including sit-stands, ramps, and stairs). However, optimizing over hundreds of nonintuitive torque bases made this method susceptible to overfitting the training data and impractical to tune for more effective assistance—experiments demonstrated inconsistent muscle effort reductions across tasks, with a particular penalty for the hamstrings.

In summary, the exoskeleton field has crucial gaps related to the LLC use case and task-agnostic control in general. Prior devices are not sufficiently versatile to reduce contributions to quadriceps fatigue over multiterrain LLC, and they have unknown efficacy at mitigating the effects of fatigue during LL tasks, when most injuries occur. Furthermore, emerging task-agnostic control methods lack interpretable parameters to customize their benefits for specific use cases and, more generally, lack predictability and safety guarantees outside of their training distribution. This paper addresses these gaps with an energy-based control strategy implemented on a highly backdrivable, bilateral knee exoskeleton (M-BLUE) to deliver safe, versatile assistance to the quadriceps across multiterrain LLC tasks (Fig. 1). The controller uses phase- and task-sensitive signals to modulate a minimal set of intuitive, predictable, and bounded torque basis functions corresponding to gravity and inertia compensation and virtual springs and dampers (Fig. 2). The associated parameters are amenable to both data-driven optimization for biomimetic assistance and subsequent application-specific tuning, for example, maximizing quadriceps assistance across LLC tasks. The quasidirect drive actuators of the M-BLUE knee exoskeleton (*48*) enable this controller to augment voluntary motion with meaningful output torques yet minimal backdrive torques. Experiments with 10 (nondisabled) participants tested our hypotheses that this versatile knee exoskeleton would (i) reduce quadriceps effort across multiterrain LLC tasks in a nonfatigued state, (ii) mitigate performance deficits during highly fatigued repetitive LL when squatting posture is enforced, and (iii) facilitate seamless task transitions (without specific training data) and garner high effectiveness rating postfatigue over a multiterrain circuit. The results indicate that this exoskeleton control framework can serve as a foundation for targeting critical muscles across multiple tasks, specifically mitigating quadriceps fatigue and its deleterious effects.

RESULTS

Our multiterrain LLC controller adapts to tasks on the basis of heuristic modification and modulation of several torque basis functions corresponding to gravity and inertia compensation and virtual springs and dampers (see control diagram in Fig. 2 and associated details in Materials and Methods). The coefficients of the basis functions were first chosen using data-driven optimization to match controller torques (given reference human kinematic/GRF inputs) to scaled reference human torques over multiple tasks as done in

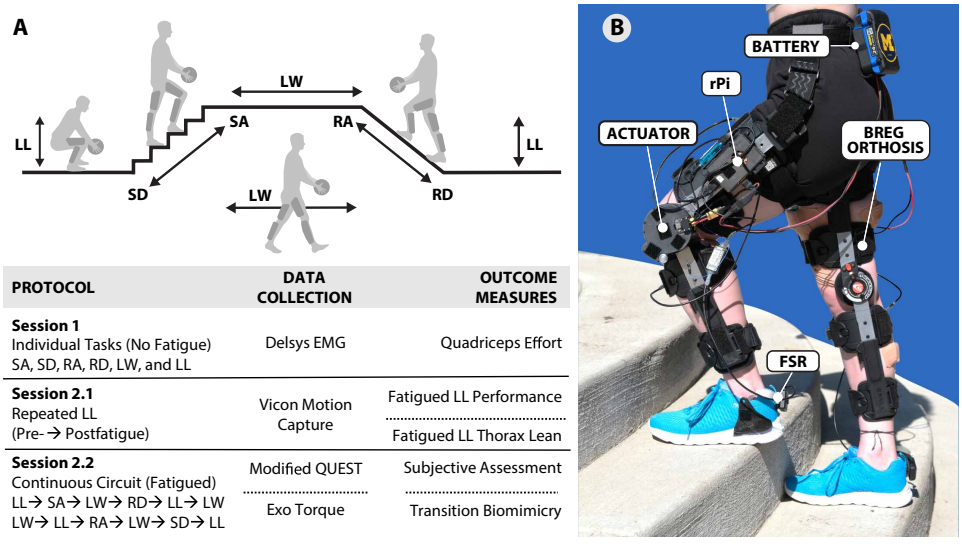

PROTOCOL	DATA COLLECTION	OUTCOME MEASURES
Session 1 Individual Tasks (No Fatigue) SA, SD, RA, RD, LW, and LL	Delsys EMG	Quadriceps Effort
Session 2.1 Repeated LL (Pre-→ Postfatigue)	Vicon Motion Capture	Fatigued LL Performance Fatigued LL Thorax Lean
Session 2.2 Continuous Circuit (Fatigued) LL→ SA→ LW→ RD→ LL→ LW LW→ LL→ RA→ LW→ SD→ LL	Modified QUEST Exo Torque	Subjective Assessment Transition Biomimicry

Fig. 1. Experimental protocol summary and M-BLUE bilateral knee exoskeleton. (**A**) Summary of protocol, data collection, and outcome measures of the two sessions. The protocol was repeated for two conditions: with exoskeleton (exo) and without exoskeleton (no-exo). In session 1, quadriceps and hamstring efforts were assessed with surface EMG for six tasks: SA, SD, RA, RD, LW, and LL. In session 2.1, fatigue mitigation was assessed during repetitive LL via time trial performance and thorax lean metrics. The fatiguing portion of the exo condition was performed with the exoskeleton in passive mode, whereas the postfatigue portion was performed with exoskeleton assistance activated. In session 2.2, continuous circuit traversal demonstrated the exoskeleton's capability to adapt assistance torque during task transitions and assessed user perception with a modified QUEST survey. (**B**) Bilateral knee modules of the modular backdrivable lower-limb unloading exoskeleton, M-BLUE. Each module comprises a highly backdrivable actuator (T-Motor AK80-9 with Dephy motor driver) retrofitted onto a commercial BREG knee brace, along with a Raspberry Pi–embedded computer, 24-V power tool battery, and force-sensitive resistor system.

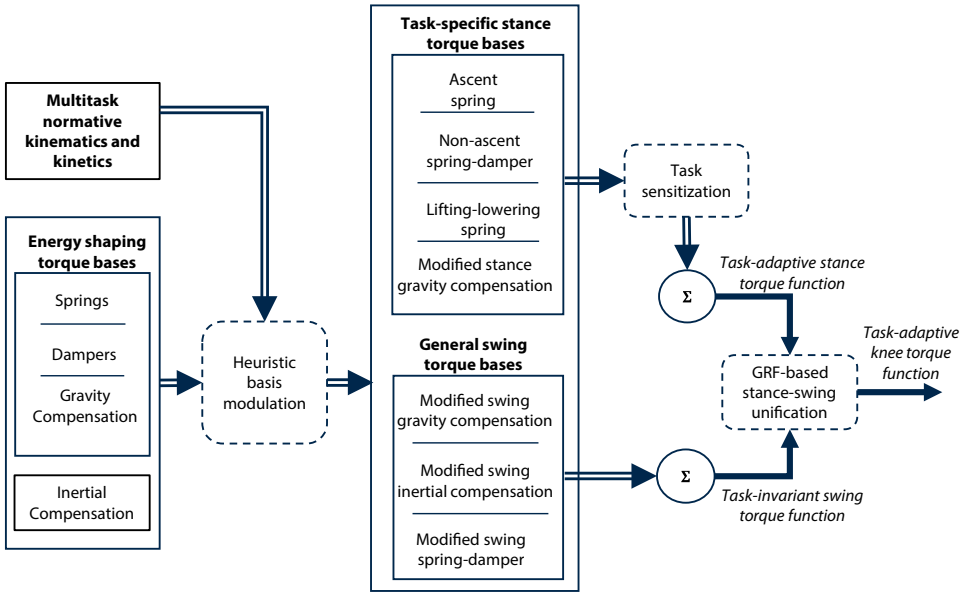

Fig. 2. Control diagram. The diagram shows a high-level summary of the process of creating the task-adaptive knee torque function. First, core energy-shaping torque bases were heuristically modified to form task-specific stance torque bases and general (task-invariant) swing torque bases. Next, for stance, task sensitization or multiplication with functions sensitive to certain task characteristics (such as terrain slope) provided task-adaptive stance torque functions. Last, taking the convex sum of the stance and swing torque bases on the basis of the GRF unifies them into the final task-adaptive knee torque function.

(*57*). The optimized controller torques match the reference human torques well in fig. S1 (see table S1 for goodness-of-fit results), demonstrating the general capability to assist squatting, LW, RA, ramp descent (RD), stair ascent (SA), and stair descent (SD), including multiple speed and incline conditions, without explicit task classification. This controller was then implemented on an improved, bilateral version of our highly backdrivable M-BLUE knee exoskeleton (9:1 gear ratio, 25-Nm peak output torque, <2-Nm peak backdrive torque) shown in Fig. 1B and detailed in Materials and Methods. The optimized coefficients provided a starting point for a manual tuning process to maximize quadriceps assistance on the basis of subjective feedback and EMG measurements in pilot testing (see Materials and Methods). After a satisfactory controller was obtained, the same set of coefficients was used for all participants ($n = 10$) in this study; no user-specific calibration was needed.

The study comprised two sessions: nonfatiguing and fatiguing—see Fig. 1A and Movie 1 for a depiction of the methods. Session 1 tested the hypothesis that the exoskeleton reduces quadriceps effort during individual LL and multiterrain carrying tasks in a nonfatigued state. At least 1 week apart, session 2 tested the hypothesis that the exoskeleton mitigates the fatigue-induced LL performance deficit (in a time trial of 10 fatigued LL reps) compared with no exoskeleton when squatting posture is enforced. Performance in a time trial is one of the classical measures of fatigue (*3*) and has been previously used to study the efficacy of back exoskeletons (*58*). Participants performed repeated squat LL until fatigue-induced failure (without power in the exoskeleton condition), immediately followed by 10 timed squat LL cycles (with power in the exoskeleton condition). Participants were instructed to take the minimum required pause between repetitions to complete the next repetition with good squat posture, emulating a typical time trial while ensuring safe posture. Although squatting posture was an experimental control, we performed an exploratory analysis of peak sagittal thorax lean to see whether the exoskeleton helped participants maintain a better squat form. After each fatiguing LL trial, participants continuously traversed a multiterrain LLC

circuit to demonstrate task adaptation and gather subjective feedback for exoskeleton effectiveness in a fatigued state.

For all metrics, we used linear mixed models with condition (no-exo, exo) and sex (male, female) as fixed effects and participant as a random effect. For postfatigue performance and posture metrics, we included additional effects of order (for the no-exo versus exo condition) and prefatigue workload (number of prefatigue LL repetitions required to reach fatigue). Sex, order, and workload were found to be nonsignificant factors in all statistical tests reported below.

Knee muscular effort and exoskeleton torques in nonfatigued LLC

We estimated quadriceps effort during six different LLC tasks (LL, LW, RA, RD, SA, and SD) for the no-exo and exo conditions in a nonfatigued state. Muscle effort was calculated as the mean root mean square EMG, normalized to % maximum voluntary contraction (%MVC), over the gait/task cycle. Quadriceps effort was estimated by taking the weighted mean of the efforts of the vastus medialis oblique (VMO), vastus lateralis (VL), and rectus femoris (RF) based on their respective physiological cross-sectional areas as per (*59*). The results confirmed our hypothesis that the knee exoskeleton reduces quadriceps effort during nonfatigued, multiterrain LLC tasks, with the caveat of LW having a nonsignificant reduction. Compared with no-exo, the exoskeleton reduced quadriceps effort for all tasks by 14.5% on average. The effort reductions were significant for all tasks except for LW, as summarized in Table 1. Figure 3 shows the distributions of quadriceps effort for all cases.

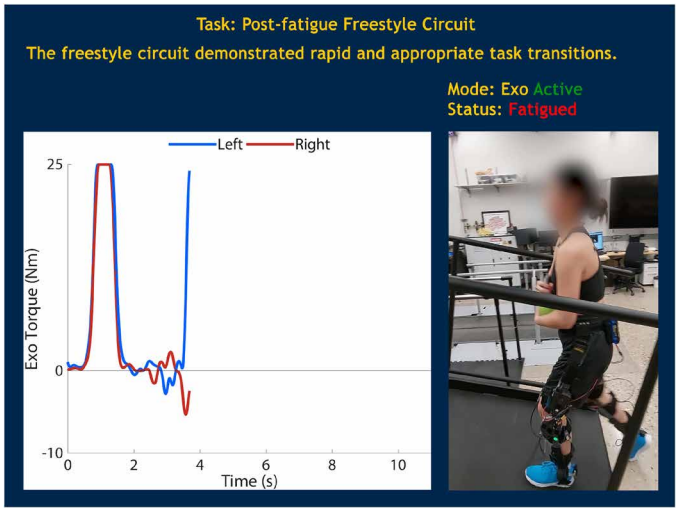

Movie 1. Summary of study results, including demonstration of real-time task adaptation of exoskeleton torques.

These results can be explained by the qualitative match between the ensemble-averaged quadriceps EMG profiles and the exoskeleton torque profiles in Fig. 3, demonstrating the appropriate timing and magnitude of the assistance torque. Furthermore, figs. S2 to S4 show trends similar to those of the individual quadriceps muscle profiles (for the VMO, VL, and RF, respectively). Averaged across all tasks, the VMO, VL, and RF efforts were 15, 14, and 11% lower, respectively, with the presented exoskeleton/controller compared with no-exo. Because our prior work found that a different exoskeleton/controller caused high hamstring activation in late stance (*57*, *60*), we also explored hamstring EMG profiles in fig. S5 by taking the mean of the biceps femoris (BF) and semitendinosus (ST) recordings. Averaged across all tasks, the mean hamstring effort was 7% lower with the presented exoskeleton/controller compared with no-exo, indicating that there was not an antagonistic penalty to the quadriceps effort reductions.

Performance and postural benefits in postfatigue LL

The results confirmed our hypothesis that the knee exoskeleton decreases the postfatigue LL performance deficit. Compared with no-exo, the bilateral knee exoskeleton induced a significant ($P < 0.01$) 43% reduction in the postfatigue time deficit, 95% confidence interval (CI) [23%, 63%], corresponding to 44% (no-exo) and 1% (exo) increases in postfatigue completion times with respect to prefatigue no-exo completion time. For no-exo and exo conditions, Fig. 4A shows the distribution of percentage completion time increases (performance deficits), and Fig. 4B shows the ensemble-averaged repetition durations over percentage trial progression (pre- to postfatigue). We also found that the prefatigue workload % (number of prefatigue LL repetitions performed in the exo condition as a percentage of the no-exo condition) was uncorrelated ($r = 0.34$) with the postfatigue completion time percentage (exo condition as a percentage of no-exo condition; fig. S6). Hence, although the exo condition required fewer repetitions to reach fatigue than no-exo, this did not bias the postfatigue results.

Compared with no-exo, the bilateral knee exoskeleton also induced a significant ($P < 0.01$) 4.4° reduction, 95% CI [2.1°, 6.6°], in peak thorax lean deviation (from the minimum lean angle in the no-exo prefatigue trial) during postfatigue LL. This corresponds to average deviations of 10.4° (no-exo) and 6.1° (exo) and average

Table 1. Quadriceps effort reductions with exoskeleton assistance. For each task, mean percentage reductions in quadriceps effort are provided—a positive value indicates that the effort with exo was lower compared with that with no-exo. The lower and upper 95% CIs for percentage reductions in effort are shown next. Last, the Holm-Bonferroni–corrected *P* value is given.

Task	Effort reduction (%)	Lower CI (%)	Upper CI (%)	*P* value
LL	22	10	32	0.0112
RA	17	10	24	0.0042
SA	24	12	34	0.0095
RD	10	3	16	0.0366
SD	11	2	18	0.0362
LW	3	−17	19	0.7490

absolute peak thorax lean angles of 53.3° (no-exo) and 48.9° (exo). Figure 4C shows the postfatigue thorax lean deviation distribution for both conditions, and Fig. 4D shows the ensemble-averaged deviations over percentage trial progression (pre- to postfatigue). Figure S7 shows deviations in peak knee flexion angles from their maximum values observed in the prefatigue phase of the respective conditions. The fatiguing phase of the trial (−100 to 0%) reveals a progressive increase in peak thorax lean (and a corresponding

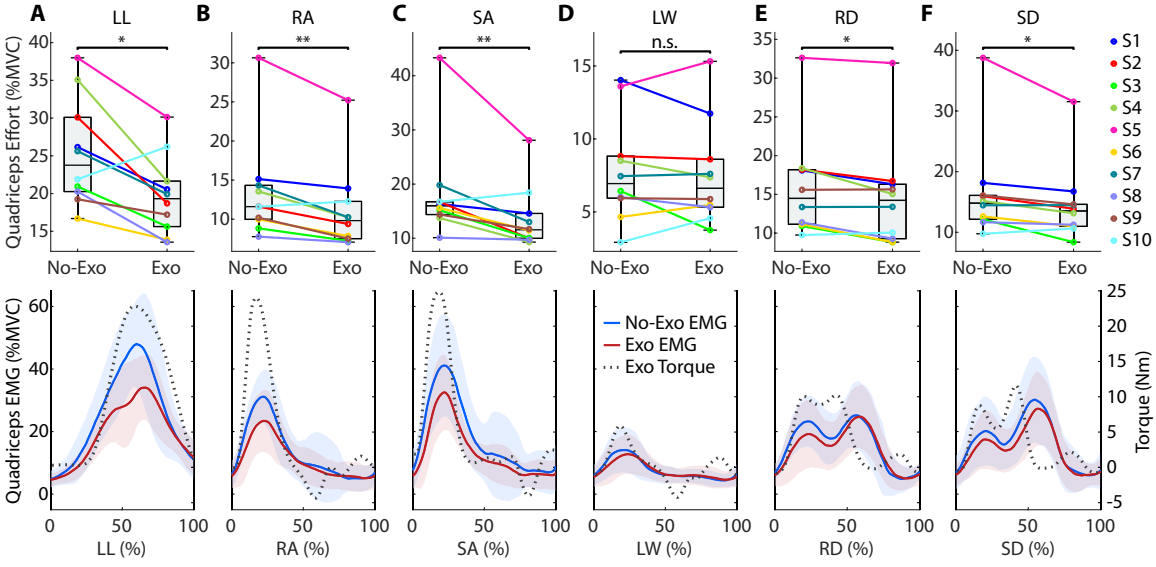

Fig. 3. Effect of exoskeleton assistance on quadriceps activation during LLC. (**A** to **F**) No-exo and exo comparisons of quadriceps effort (top) and activation profiles (bottom) for the six LLC tasks tested. For each task, the box plots and individual line plots show the distributions of quadriceps effort [weighted mean of VMO, RF, and VL according to respective physiological cross-sectional areas (*59*)]. Results for tasks other than LW were generally consistent across participants except for S10, who was the heaviest participant and thus received the least benefit from the exo relative to body mass; * represents a statistically significant difference ($P < 0.05$) as per our linear mixed model with $n = 10$; **$P \leq 0.01$; n.s., not significant. The ensemble-averaged quadriceps EMG profiles show general alignment with the exo assistance torque (dashed curve, positive for extension). The shaded regions represent ±1 standard deviation about the mean activation.

Fig. 4. Mitigation of fatigue-induced performance deficit and thorax lean deviation. (**A**) For the no-exo and exo conditions, box plots and individual line plots show the percentage increase (performance deficit) in time to complete 10 postfatigue LL repetitions with respect to the prefatigue baseline (time to complete 10 repetitions in the prefatigue no-exo condition for each participant). (**B**) For the no-exo and exo conditions, the ensemble-averaged plots depict the pre-/postfatigue LL repetition durations over percentage trial progression [−100 to 0% represents the fatiguing phase with a variable number of repetitions for each participant and condition, 0% represents the point of fatigue declaration, and 10 to 100% represents the (fixed) 10 postfatigue LL repetitions]. The shaded regions represent ±1 standard deviation about the mean. (**C**) No-exo and exo comparisons of mean deviation in postfatigue thorax lean with respect to the prefatigue baseline (minimum thorax lean angle observed in the prefatigue no-exo condition for each participant). Larger values indicate more thorax lean (stooping). (**D**) No-exo and exo comparisons of pre-/postfatigue thorax lean deviation from prefatigue baseline over percentage trial progression. ** represents a statistically significant difference ($P \leq 0.01$) as per our linear mixed model with $n = 10$.

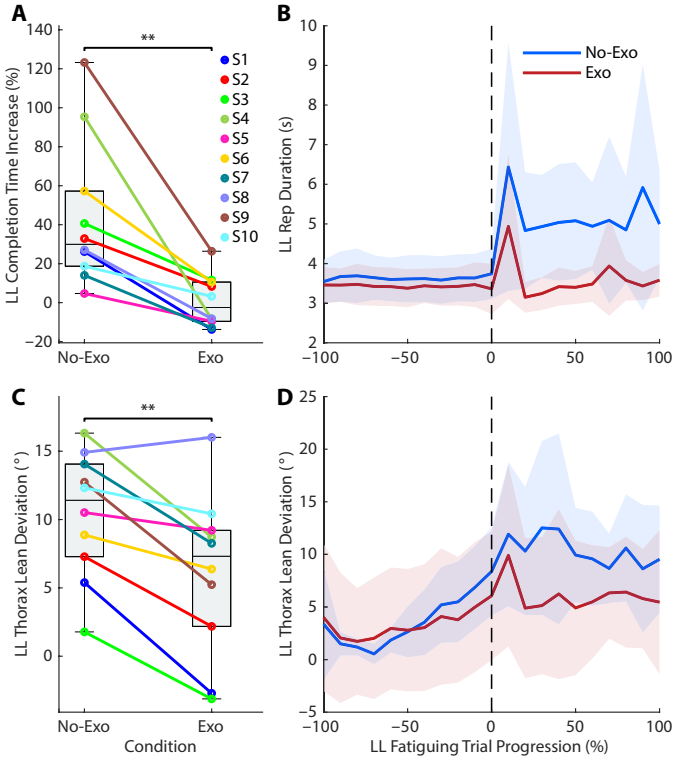

decrease in peak knee flexion angles), with similar slopes and relative magnitudes between the exo and no-exo conditions. After the onset of exoskeleton assistance (>0% trial progression), the thorax lean trajectories for the two conditions diverge, where the exo condition tends to return to prefatigue levels—a similar but less marked trend can be observed with the peak knee flexion angles, which were (4 ± 13)° higher postfatigue with exo compared with no-exo. Last, the ensemble-averaged thorax lean profiles in fig. S8 verified that the peaks in the thorax lean occurred at the bottom of the squat LL cycles as expected.

Task adaptation and effectiveness ratings during continuous LLC

The exoskeleton torques rapidly and appropriately adapted to varied terrains over the multiterrain circuit. Focusing on the transition strides, the across-participant average exoskeleton torques resemble scaled human torques in Fig. 5, despite the controller not being trained on transition data. Moreover, Fig. 6 shows important exoskeleton signals and the resulting assistance torque as a representative participant continuously traversed the circuit. Task-sensitive signals δ_{AJCy} and $\delta_{AJCdist}$ (defined in Fig. 6 and fig. S9) change instantly at first contact with new terrain, causing instant torque adaptation (within 7 ms after contact detection) followed by consistent behavior during each steady-state activity. In particular, $\delta_{AJCdist}$ goes low during stationary tasks (activating the LL virtual spring), and δ_{AJCy} goes high during ascent tasks and low during descent tasks (activating the respective virtual spring). These signals trigger appropriate changes in assistive torque and power, delivering more positive work during ascent tasks and negative work during descent tasks.

The average participant rating for exoskeleton effectiveness across these multiterrain LLC tasks (postfatigue) was 4.3 out of 5 on the modified Quebec User Evaluation of Satisfaction with Assistive Technology (QUEST) survey (*61*). The individual task averages were 4.8 for LL, 4.8 for SA, 4.3 for SD, 4.2 for RA, 4.2 for RD, and 3.6 for LW. See Fig. 7 for the distribution of ratings for the tasks.

DISCUSSION

State-of-the-art exoskeletons and their control strategies lack the versatility and customizability to target the critically involved quadriceps during multiterrain LLC, which comprise varied tasks including high-torque closed-chain squatting as well as open-chain gait tasks such as LW, ramps, and stairs (see table S2 for a summary of state-of-the-art LLC controllers). In particular, prior LLC studies have not demonstrated holistic (multiterrain) and multifaceted (muscular, performance, postural, and perceptual) exoskeleton benefits, especially in highly fatigued states, which are correlated with injuries during LL. This paper addresses these gaps with a versatile energy-based control strategy (see Materials and Methods), which was first optimized to provide a foundational assistive controller (matching reference human torques in silico in fig. S1 and table S1) and then customized to maximize quadriceps assistance during multiterrain LLC (matching quadriceps activations in vivo in Fig. 3). When deployed on a backdrivable knee exoskeleton, the assistance torques provided holistic reductions in quadriceps effort (Fig. 3) during multiterrain LLC in nonfatigued conditions, significant performance and postural benefits to squat LL in a highly fatigued condition (Fig. 4), and rapid and appropriate adaptation during task transitions (Figs. 5 and 6) with high effectiveness rating postfatigue on a multiterrain circuit.

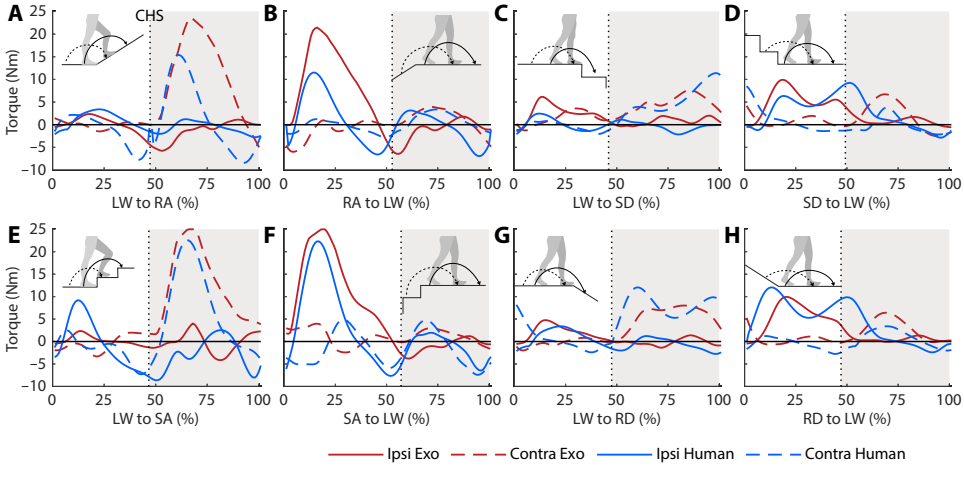

Fig. 5. Exoskeleton torque during task transitions. (**A** to **H**) Exoskeleton commanded torques of the ipsilateral leg (reference side) are shown in solid red, and the contralateral leg is shown in dashed red for the transition strides averaged across participants for eight transition types. Corresponding biological torques for an 80-kg person (*62*, *63*) are shown as blue lines, where SD and RD are scaled down to 10%, and other tasks are scaled down to 25% to match assistance levels used (on the basis of user feedback during pilot testing). Note that 0 and 100% on the *x* axes represent subsequent ipsilateral heelstrikes. The trailing stride is shown for all transitions except the LW to SD/RD transitions, for which the leading strides are shown—refer to (*63*) for stride definitions. The swing portion of the controller is task invariant. Instant adaptation of stance exoskeleton torque can be observed at contralateral heelstrike (CHS), denoted with a vertical dotted line. The stance torque of the ipsilateral leg (solid red 0 to 60%) is suited for the previous terrain, and the stance torque of the contralateral leg (dashed red after CHS) is suited for the new terrain. The illustrations depict the point of the CHS, where the dashed arc is the contralateral footpath, and the solid arc is the ipsilateral footpath.

Task-adaptive knee exoskeleton reduces quadriceps effort in multiterrain LLC

We found a holistic decrease in quadriceps effort (without negatively affecting the antagonistic hamstrings) across all LLC tasks in the nonfatigued session (Fig. 3). One of the main factors in these consistent findings could be our mixed in silico and in vivo approach to the controller development, whereas prior task-agnostic controllers (including our prior work) were limited by and restricted to the human dataset that informed their data-driven training processes (*53*, *54*, *57*). For example, the training data (*62*) used in our initial optimization lacked sufficient flexion torque during late stance [diverging from other datasets such as (*63*, *64*)], which we resolved through in vivo controller tuning (see Supplementary Methods).

The peaks in assistive torques are well aligned with the peaks in quadriceps activations across tasks in Fig. 3,

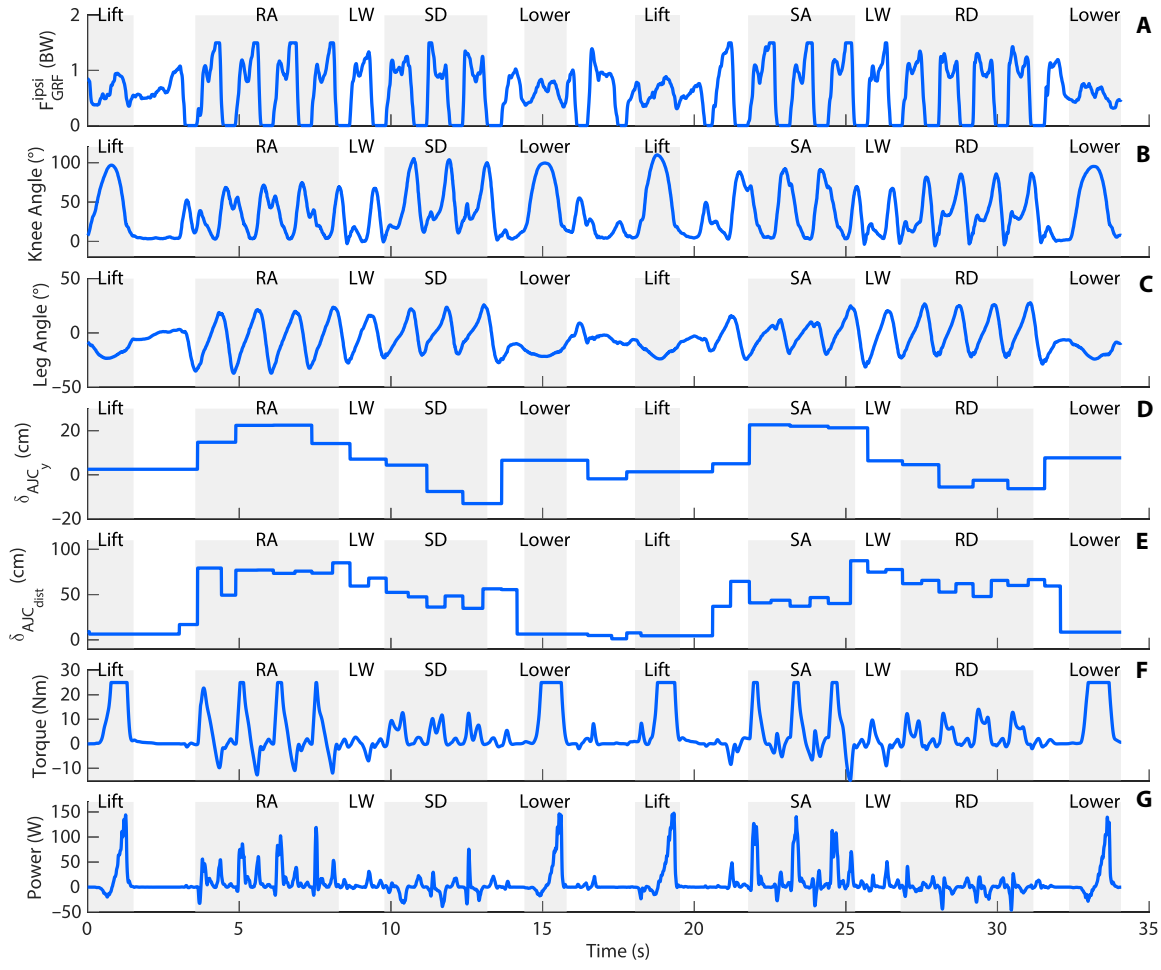

Fig. 6. Important exoskeleton signals during continuous LLC over the multiterrain circuit. (**A** to **G**) Seven important signals of the right knee exoskeleton module during a representative participant's continuous circuit traversal trial in session 2.2 are shown—see Supplementary Methods for a detailed description of each signal. Briefly, F^{ipsi}_{GRF} shows the GRF sensed by the right foot's insole, which is approximately 0 body weight (BW) during swing, 0.5 BW during double support (such as during LL), and 1 BW during single support stance. The knee angle is the difference between the sagittal angles of the thigh and shank inertial measurement units (flexion is positive, and 0 represents the angle in the anatomical standing position). The leg angle (pseudophase variable) provides an estimate of gait cycle progression whereby 0 represents standing, and a positive angle is observed when the hip joint center is anterior to the ankle joint center. The vertical difference between the bilateral ankle joint centers (δ_{AJCy}) is used to update the estimate of terrain inclination at heelstrike, in turn, modulating activation of the ascent and nonascent springs (as seen in the torque plot). The distance between the bilateral ankle joint centers at heelstrike ($\delta_{AJCdist}$) is used to estimate the symmetry between the two limbs, in turn, modulating activation of the LL spring (fully active for low δ_{AJCy}). The task-adaptive knee exoskeleton torque (positive for extension) is shown next. Last, the power delivered by the exoskeleton is shown in the last panel, which is predominantly positive except for the descent tasks (including the first part of LL) as expected.

explaining the significant reductions in quadriceps effort in the exo condition (except for LW). It should be noted that human muscles are much more efficient in performing negative work (as required in descent tasks) compared with positive work (required in ascent tasks). It is, therefore, understandable that participants found the assistive torques the most helpful in the tasks requiring high positive work (Fig. 7). SA, LL, and RA had the highest reductions in quadriceps effort. On the other hand, the knee exoskeleton was the least effective at assisting LW. This task received the lowest effectiveness rating postfatigue (3.6 of 5) and was also the only task that had a nonsignificant decrease in quadriceps effort with exoskeleton assistance. This result can be explained by the fact that LW exhibits the lowest knee moments out of all tasks (fig. S1) and accordingly received the lowest assistance torque magnitude (Fig. 3). These assistive torques were well aligned to the quadriceps activation profile, but we suspect that soft tissue compliance prevented effective energy transfer from the relatively smaller exoskeleton torques associated with LW. Fortunately, the presented exoskeleton/controller satisfactorily eliminated the high peaks in late-stance hamstring activation seen in our prior studies (*57*, *60*), likely as a result of adding knee flexion torques via gravity compensation and using a significantly lighter exoskeleton. In summary, the exoskeleton successfully reduced quadriceps effort in the quadriceps-intensive tasks that contribute most to muscular fatigue without an observed penalty.

Quadriceps assistance mitigates fatigue-induced LL performance and posture deficits

Fatigue is inevitable in physically demanding jobs and is a causal factor for work-related musculoskeletal disorders (*1*). Our results

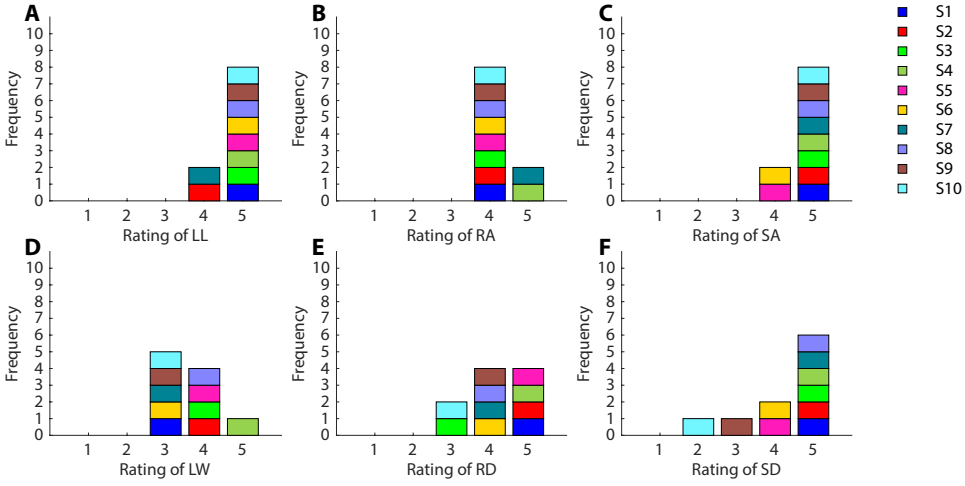

Fig. 7. Modified QUEST summary. (**A** to **F**) Stacked histograms show the individual results of the modified QUEST for the six postfatigue tasks of LL, RA, SA, LW, RD, and SD. The tasks were performed as part of the continuous circuit. The participants rated their satisfaction with the exoskeleton assistance on a scale of 1, not satisfied at all; 2, not very satisfied; 3, more or less satisfied; 4, quite satisfied; and 5, very satisfied.

demonstrate that the exoskeleton can mitigate the deleterious effects of fatigue on LL performance (*2*) and posture (*23*), which has implications for injury risk. Neuromuscular fatigue can be quantified by the decrease in the muscle's peak force production ability (or peak torque of the corresponding joint). The peak knee torque for a fast squat is about 1.4 Nm kg^{-1} (*65*), or about 100 Nm for an average person. During the fast LL squats performed in our study, the peak knee torque is required at the bottom of the squat to redirect the body's downward momentum upward. The bottom of the squat is also where we observed the peak in postfatigue thorax lean (fig. S8), a likely consequence of participants trying to reduce the moment arm on the knee (and stress on the fatigued quadriceps) in this biomechanically compromised position. The peak of the exoskeleton torque profile was well aligned with this high-torque squat phase (providing about 25% of biological torque), resulting in good alignment with the quadriceps EMG peaks (Fig. 3). Accordingly, exoskeleton assistance yielded a 22% reduction in mean quadriceps effort and a 23% decrease in peak activation for nonfatigued LL. This result is in line with the ~18% reduction in quadriceps activation during lowering in (*49*) but differs from the 60% reduction found with just 16-Nm peak assistance torque in (*66*). However, the participants in (*66*) had a highly bent-over posture during the squat lifts, suggesting that a much lower net knee extension torque was required for their task (for which 16 Nm is a higher percentage).

A fatiguing squat study reported a 25% decline in maximal quadriceps force after fatiguing exercises (*67*), but we did not measure maximal quadriceps forces pre- and postfatigue in our study. If we make relatively broad assumptions of a linear relationship between EMG and force (*68*) and consider fast LL as a maximal activity for the quadriceps, then the 23% savings in peak quadriceps force afforded by the exoskeleton was likely sufficient to fully overcome the supposed 25% deficit in force from the induced fatigue. This could explain how the exoskeleton assistance enabled the participants to significantly reduce their fatigue-induced deficit in time to complete 10 LL repetitions by 43% and with significantly better posture (4.4° decrease in global thorax angle) compared with the no-exo condition. The exoskeleton assistance limited the fatigue-induced time deficit to a mere 1% increase relative to prefatigue levels. On the other hand, the LL durations in the no-exo condition increased substantially postfatigue, indicating a persistent fatigue-induced performance deficit. The mean LL repetition durations before declaring fatigue were quite similar for both the no-exo and (passive) exo conditions, suggesting similar levels of fatigue. After participants declared fatigue, both conditions had a peak LL duration at the first repetition because this was when they experienced peak fatigue. Participants were instructed to pause just long enough to be able to continue with proper squat form during postfatigue repetitions; the first pause allowed recovery to a fatigue level marginally below failure, which was maintained over subsequent repetitions. The exo condition likely had a smaller pause because participants had more confidence continuing after fatigue when assistance was expected. The postfatigue LL feedback rating of 4.8 was also the highest among the tasks (almost a perfect 5 out of 5), supporting the effectiveness of the exoskeleton assistance at a perceptual level.

The exoskeleton's replenishment of the diminished quadriceps force in postfatigue LL explains the significant reduction in peak thorax lean (amount of stooping) for the exo condition compared with the no-exo condition. A similar rate and magnitude of increase in peak thorax lean were observed between the no-exo and (passive) exo conditions in the fatiguing phase of the trial (−100 to 0% trial progression in Fig. 4D), indicating similar intensities of fatigue. This observation agrees with a classic study showing that quadriceps fatigue leads to a compensatory change in posture (more stooping) (*23*). Upon the onset of exoskeleton assistance (>0% trial progression), the peak thorax lean returns quickly (within two postfatigue repetitions) toward a prefatigue level, indicating mitigation of fatigue. In contrast, the no-exo condition continues to gradually increase (reaching its highest point at the third postfatigue repetition) before leveling off at a noticeably higher value than the prefatigue level, suggesting retention of high-fatigue postural effects. Without assistance, the participants likely offloaded their highly fatigued quadriceps by leaning forward and thus reducing the moment arm on their knees. In contrast, exoskeleton assistance enabled participants to use more of their legs, thus precluding stooping—this can be observed in the ensemble average deviation in peak knee flexion angle in fig. S7. Moreover, although fatigue decreases peak knee flexion (hence also knee range of motion) at similar rates and magnitudes in both conditions (−100 to 0% trial progression), exoskeleton assistance partially recovered the loss in the range of motion (>0% trial progression), allowing for a straighter and safer back posture.

The observed changes in posture were likely subconscious phenomena because participants were reminded to (i) maintain proper squat posture during the fatiguing portion and (ii) take a longer pause if they perceived an imminent compromise in posture during the postfatigue portion. This likely resembles real workplace scenarios, where fatigue-induced injurious changes in

posture occur subconsciously to override worker training and guidelines. Our study showed a partial reversal of compensatory changes in posture via exoskeleton assistance. This intervention addresses the root cause of postural changes (fatigued quadriceps) rather than simply alerting the user by means of a vibrator as in (*69*).

Study limitations

A possible limitation of this study was relying on participants' perception of their point of failure to control the level of fatigue between no-exo and exo conditions. However, the self-assessed failure point, identified by a disproportionately large increase in effort to complete the desired movement with proper form, is commonly used in resistance training (*70*) and fitness tests (*71*). EMG has been used to estimate neuromuscular fatigue offline with mixed results (*72*), but real-time assessment to declare fatigue would have been impractical. Nevertheless, the similarities between conditions in repetition durations (Fig. 4B), thorax angle (Fig. 4D), and knee angle (fig. S7) leading up to fatigue (−100 to 0% trial progressions) suggest that the participants reached similar levels of fatigue at failure.

In addition, the two fatiguing conditions (no-exo and exo) were performed on the same day (session 2), potentially causing greater fatigue for the second condition. This study design was intended to make it easier for participants to declare fatigue at a similar point of failure. To minimize the possible confound, we gave participants ample time to rest between conditions and alternated the order of conditions between participants. Moreover, the effect of the order was nonsignificant in explaining the postfatigue performance and posture outcomes.

Although the observed reductions in quadriceps effort did not have an associated penalty with the hamstrings, we did not study associated changes in other leg muscles or overall metabolic cost. It is worth noting that the RF (fig. S4) serves as both a knee extensor and hip flexor and that the hamstrings (fig. S5) serve as both knee flexors and hip extensors, giving some insight into the hip effort. Even if other muscles had increased effort, they are less susceptible to fatigue than the quadriceps in squat LL (*22*) and ramp/stair (*31*) tasks. By focusing on quadriceps effort, the presented knee exoskeleton improved LL posture and performance and received high subjective scores during continuous LLC trials. However, we did not examine cumulative activation of the quadriceps during these continuous trials, which is left to future work.

Future work

The significant reduction in quadriceps EMG during nonfatigued LL suggests that the exoskeleton could also delay the onset of fatigue, which could be studied with an endurance test until failure. Future work could also integrate the presented knee exoskeleton with a hip-back brace to directly offload the lower back, helping workers lift loads that cannot be placed between the feet (because of their shape or size). Furthermore, hip and/or ankle assistance may be necessary during frequent level-ground carrying, where a knee exoskeleton alone offers little benefit. The inherently modular nature of the knee exoskeleton presented in this study allows it to be readily interfaced with a hip-back and/or ankle exoskeleton to provide versatile assistance for LLC tasks, including stooping. We presented a modular knee-hip combination of our exoskeleton in prior work, albeit only performing a single LL task with a simple gravity-shaping controller (*48*).

In future work, we hope to extend the control approach developed here to combinations of hip-knee-ankle modules and test their efficacy in continuous LLC with various types of loads. Furthermore, additional tasks could be supported by the presented control methods, such as backward hauling of loaded trolleys/dollies up stairs and ramps. The customizable controller can also be extended to general-purpose assistance for mobility-limited individuals, such as the elderly, by modifying the LL spring for sit-stand tasks. The coefficients for the three types of springs and gravity compensation can be safely and independently tuned, enabling future customization to unique gait impairments. This control approach is also amenable to personalization via human-in-the-loop optimization, which requires a small set of tunable parameters (*42*, *55*).

Conclusion

The presented knee exoskeleton and the controller provided versatile assistance across multiterrain LLC tasks, effectively mitigating quadriceps fatigue. These results suggest that knee exoskeletons could be deployed in physically demanding workplaces to reduce fatigue, enhance lifting performance, and potentially reduce the risk of lower back injuries. This control framework also addresses fundamental limitations with emerging task-agnostic exoskeleton controllers, which typically lack interpretability, customizability, safety guarantees, predictability, and/or responsiveness during transitions. Achieving biomimetic torque prediction via data-driven optimization provides a general foundation from which the small set of intuitive parameters can be customized for personalized assistance or different use cases, including elderly assistance or specific gait impairments.

MATERIALS AND METHODS

Controller overview

Our control objective was to safely, rapidly, and appropriately adapt exoskeleton assistance torque across several common activities, specifically tailored to reducing quadriceps effort during multiterrain LLC. To make the controller stable and predictable, we took inspiration from the energy-shaping framework previously used to design energetically passive controllers within the stance or swing phase (*73*). Instead of tracking reference trajectories, this style of controller can generate torques to augment the mechanical energy of the coupled human-exoskeleton system in a manner that assists various activities (for example, compensating gravity and/or inertia). A theoretical guarantee of passivity ensures that the exoskeleton cannot inject net positive energy over a cycle between identical leg configurations, with the exception of instantaneous changes in potential energy when switching between distinct stance and swing controllers. This further implies that the human retains control over net energy growth and that the exoskeleton cannot cause unstable energy injection or oscillations. This guarantee is particularly important when operating outside the controller's design/training conditions (*74*), whereas emerging neural network–based approaches such as in (*54*) are inherently unpredictable in such circumstances.

However, strict energetic passivity only allows energy injection when switching between stance and swing controllers (for example, changing the equilibrium angle of a virtual spring), which precludes

continuous energy injection throughout the stride. We therefore relaxed the passivity requirement in our controller design to permit both small continuous injections and large event-based injections of energy as in (*57*). As an example of the former, we used a gravity compensation term at the knee that depends on the global angle of the shank during phases of underactuation (*57*). As an example of the latter, a preloaded ascent spring activates when the foot touches down to propel the user up stairs or on ramps, where the amount of energy injection is a predictable function of the initial knee flexion angle.

The approach in (*57*) relies on purely data-driven optimization to choose dozens of unintuitive controller parameters, which are difficult to adjust for different use cases like LLC. To build an intuitive and customizable controller (depicted in Fig. 2), we began with a short list of physical, bounded components that obey the assumptions of (*57*). These components include springs, dampers, inertia compensation, and gravity compensation, and because each one maps from measurable quantities to torque, they can serve as basis functions to parameterize the control law. We then deviated from the energy shaping framework (*57*) by heuristically modulating these core torque bases into specialized task- and phase-specific behaviors. We obtained task-specific stance torque bases (for example, ascent spring) that are suitable for specific task categories (for example, incline walking) and general swing torque bases (for example, modified gravity compensation) that are universally helpful in swing (in other words, task-invariant). A part of this specialization involves "phase sensitization" using a robust phase variable (*75*), which, for example, suppresses the ascent spring in late stance that would otherwise hinder the transition to swing.

Next, the process of "task sensitization" modulates the specialized stance torque basis functions to accommodate differences between activities and variations within activities. For example, the ascent spring injects net positive energy only for incline or up-stair tasks (with higher energy injected for steeper inclines), and a nonascent spring damper absorbs energy only for decline, down-stair, and LW tasks. Essentially, task sensitization involves scaling the specialized basis functions by smooth functions of task-sensitive signals (for example, the height differential between the two ankle joint centers at heel-strike, which is sensitive to terrain incline). Summing the task-sensitized stance basis functions gives the task-adaptive stance torque function, which is parameterized fully by kinematic and GRF feedback. Last, the GRF-weighted convex combination of the task-adaptive stance torque function and task-invariant swing torque function provides the final task-adaptive knee torque. See Supplementary Methods for a detailed description of the controller and its data-driven optimization and in vivo customization, resulting in the parameters given in table S3.

Hardware/controller implementation

The controller was implemented on an improved, bilateral version of our M-BLUE knee exoskeleton module (*48*), as shown in Fig. 1B. Each module had a highly backdrivable commercial actuator (T-Motor AK80-9), comprising a high-torque pancake motor and an internal 9:1 planetary gearset. This actuator has very low reflected friction and inertia (92.1 kg·cm^2), enabling high-bandwidth torque control [42- to 60-Hz cutoff (*76*)] without a torque sensor as commonly used with higher inertia actuators [such as 691.5 kg·cm^2 in (*73*)]. In particular, the output torque of the AK80-9 actuator can be accurately modeled as a function of q-axis motor current with less than 0.39-Nm error (*48*). Therefore, tracking of the desired output torque was handled by the FASTER motor driver (Dephy, Inc.) in the current control mode. We bypassed the driver's default thermal limits and implemented a thermal model–based torque limiter that smoothly tapers the actuator torque on the basis of the estimated coil temperature (*77*), allowing short (1- to 2-s) bursts of higher peak torques (limited to 25 Nm) than the default setting. We also implemented a GRF sensor (IEE Sense) on the basis of a matrix of force-sensitive resistors. Last, we improved comfort and practicality by attaching the Raspberry Pi computation unit onboard, implemented waist-mounted "plug-and-play" power tool batteries for better familiarity with construction workers, and included a waist suspension strap to prevent exoskeleton slipping/sliding.

The Raspberry Pi–embedded computer ran a 150-Hz real-time control loop to compute the task-adaptive torque commands on the basis of sampled sensor feedback. Each torque command was converted to a q-axis motor current command [using the identified torque model from (*48*)] and sent to the motor driver over USB. Running its own low-level control loop at 10 kHz, the motor driver tracked the commanded q-axis current (and thus torque) before receiving the next command from the high-level control loop. Figure S10 depicts the current/torque tracking for a representative participant performing a continuous LLC circuit traversal. Across participants, the average root mean square error between commanded torque and estimated torque (measured current × gear ratio 9:1 × motor torque constant 0.146 Nm/A) was 0.61 Nm with a standard deviation of 0.05 Nm.

Experimental protocol

We sought to study the effects of the controller/exoskeleton on performance, posture, muscle activity, and user perception during assisted multiterrain LLC in fatigued and nonfatigued conditions (Fig. 1A). The study was approved by the Institutional Review Board at University of Michigan (HUM00201957) and associated with clinical trial number NCT05240014. Ten ($n = 10$) participants (five males, five females, age 25 ± 1 years) who had prior knowledge of and experience with the squat lifting technique completed this study (see table S4 for demographics). The experiment was divided into two sessions: nonfatiguing and fatiguing, which were completed on two separate days at least 1 week apart to provide adequate recovery time.

Before the first session, participants underwent exoskeleton acclimation for approximately 15 min, in which they traversed the multiterrain circuit until they felt comfortably attuned to the behavior of the exoskeleton. For the ascent tasks, the experimenter explained the intuitive concept of using a preloaded spring (likened to a spring-loaded toy car). For descent and LW tasks, we explained the concept of a bracing knee spring that prevents knee buckling.

Last, for the squat LL task, the concept of a velocity-dependent torsion spring was explained by likening it to intention detection. For the squat descent (negative work) portion, we explained that the knee spring would resist the user's downward motion less if it detected a stronger intention to descend (faster knee bending). For the squat ascent portion, because the direction of velocity was the same as that of the spring torque, we explained that the controller would feel similar to a conventional torsion spring.

After acclimation with the exoskeleton, we acquired important gait parameters for each participant in the no-exo condition for each portion of the circuit except LW. For ascent tasks (ramp and stairs),

we acquired the participants' maximum knee extension velocity in stance, and similarly, for descent tasks, we acquired their maximum knee flexion velocity in stance. For LL, we acquired the maximum knee extension velocity of the squat ascent portion. These parameters served as experimental controls in session 1.

Session 1 (nonfatiguing) protocol

The purpose of this session was to assess the effect of the exoskeleton on quadriceps effort in six tasks (LW, RA, RD, SA, SD, and squat LL) in a nonfatigued state. Accordingly, participants traversed each portion of the ramp/stair circuit and a 10-m level walkway multiple times until we collected at least 10 gait/task cycles for each task in which the corresponding maximum velocities in stance were within ±10% of the baseline values collected during acclimation. Because LW is relatively more common and natural than the other tasks, we did not enforce a velocity constraint and instead asked participants to walk at their self-selected speed. The tasks were repeated with both no-exo and exo conditions, with the order of the conditions alternated between subsequent participants. To emulate safe carrying etiquette, for the SD and RD tasks, participants were reminded to carefully walk and lower themselves down and not to skip or hop down. Because a variety of SA styles exist—knee-dominant (most common), hip-dominant, and ankle-dominant—it was plausible for newly acclimated participants to change their climbing style in response to the assistive knee torques, potentially confounding the EMG comparisons between conditions. We thus encouraged the participants to use the most common knee-dominant style for both conditions (during both acclimation and data collection trials), which turned out to be the natural style for all participants.

Session 2 (fatiguing) protocol

The purpose of session 2 was to assess the mitigating effect of the exoskeleton on postfatigue LL performance deficit when enforcing the squat form and to acquire a subjective assessment of its effectiveness on postfatigue multiterrain LLC. Accordingly, participants performed continuous squat LL repetitions with a 9-kg kettlebell until "failure," with no pausing allowed between repetitions. Participants were instructed to verbally declare failure when they felt they could no longer complete the next repetition with proper squat form without needing a pause. Declaring fatigue initiated a time trial of 10 fatigued LL repetitions in which participants were permitted to pause long enough after repetitions to complete the next repetition with perceived good squat form. The participants were oblivious to the timed nature of the trial and were instructed to focus their attention on their posture. This process was repeated without the exoskeleton and with the exoskeleton. The order of conditions was alternated between participants, and a minimum break of 15 min (or longer if the participant desired) was enforced between conditions. For the exoskeleton condition, the fatiguing repetitions were performed with the exoskeleton in passive mode, for which the exoskeleton has an imperceptible ~1-Nm backdrive torque for the joint accelerations encountered during LL (*48*). With the use of a wireless push button, the researcher changed the exoskeleton to active mode immediately after "fatigued" was declared by the participants, providing the participants with assistance during the postfatigue repetitions.

Immediately after completing the 10 postfatigue LL repetitions, the participants walked over a multiterrain circuit while carrying the 9-kg mass. The circuit comprised a 3.7-m ramp inclined at 15°, a short level platform of 2 m, and a five-step staircase with an 18-cm step height. The circuit was traversed in a continuous, freestyle fashion in both directions and included a squat LL repetition on both ends of the circuit to emulate a workplace multiterrain LLC scenario. Two round-trip laps of the circuit were completed for each condition. After completing the circuit with the second condition, participants rated the effectiveness of the exoskeleton assistance over the circuit by filling out a modified QUEST (*61*) questionnaire (see table S5 for the list of questions). The questionnaire gathered discretized ratings of 1 to 5 (not satisfied at all, not very satisfied, somewhat satisfied, quite satisfied, and very satisfied, respectively) for all steady-state portions of the circuit (RA, RD, SA, SD, LW, and LL). The participants only considered the effectiveness of the exoskeleton during the postfatigue circuit traversal.

Data collection

Multiterrain quadriceps effort

In session 1, after appropriate skin preparation, we secured five EMG electrodes (Trigno Avanti and Snap, Delsys, MA, USA) onto the participant's right VMO, VL, RF, BF, and ST to assess quadriceps and hamstring muscle activation. Participants performed an MVC procedure comprising explosive jump squats (eliciting maximal dynamic contraction) and maximal isometric contraction against manual resistance, which enabled EMG data to be normalized to %MVC.

To assess muscular effort, we calculated the mean of the MVC-normalized root mean square signal for each gait/task cycle. The root mean square signal provided by the Delsys EMG acquisition software was used for this purpose (window length: 125 ms, 122-ms overlap). Because we were interested in gross quadriceps effort, and to reduce the number of degrees of freedom in our statistical analysis, we took the weighted average of the three quadriceps muscles that we recorded to get a gross quadriceps effort metric. The weighting was based on the respective physiological cross-sectional area of each muscle as per (*59*).

Postfatigue LL performance deficit

Postfatigue LL performance deficit was evaluated by the percentage increase in time to complete 10 LL repetitions after the participant exclaimed "fatigued" in session 2, with respect to baseline. The baseline was determined by the time to complete the first 10 LL repetitions during the prefatigue phase in the no-exo condition for each participant. An LL repetition started with the participant standing in the upright posture without the weight, then lifting the weight from the ground and attaining the upright standing posture, lowering the weight back to the ground, and standing upright once again without the weight. Because some participants declared fatigue midway through repetition, the time measurement was started when the last fatiguing repetition was fully completed. Because pausing between repetitions was allowed in the 10 postfatigued repetitions, most participants took a 2- to 3-s pause immediately after declaring fatigue—this time was included in the time to complete metric. The time to complete analysis was performed offline using sagittal-plane video recordings.

Postfatigue LL posture deviation

Although squatting posture was an experimental control in session 2, we performed an exploratory analysis of lifting posture (peak thorax lean) to see whether the exoskeleton helped participants maintain a better squat form. A Vicon motion capture system (Oxford Metrics, Oxford, UK) was used to collect three-dimensional marker trajectories for session 2's LL trials. Retroreflective markers on the torso were placed at C7, T10, CLAV, and STRN to define the thorax segment (*78*). Three additional backup markers were placed on the shoulders and lower back to aid in postprocess gap filling. After

appropriate data cleanup, gap filling, and filtering, we calculated the sagittal plane global thorax angle with respect to upright standing (0°) (*79*). First, the peak global thorax angle was found for each lifting and lowering squat. Next, the deviation in thorax lean was calculated by subtracting the value of the lowest peak found in the prefatigue no-exo condition. Last, the mean of the deviations from 20 postfatigue squats total (10 lifts and 10 lowers) was taken for each participant and condition.

Statistical analysis

Our power analysis (for 80% power, $\alpha = 0.05$) on pilot data for LL performance and EMG returned a sample size of $n = 10$. After collecting data from all 10 participants, we first confirmed the normality of the data using QQ plots.

Quadriceps muscular effort was analyzed using a linear mixed model in MATLAB with restricted maximum likelihood estimation of parameters. Data from our 10 participants were tabulated with information comprising log-transformed quadriceps muscle effort, condition (no-exo, exo), and sex (male, female). We defined exoskeleton condition and sex as categorical variables and fit a separate linear mixed model for each task, where the condition and sex are fixed effects and the participant is a random effect

$$\text{Effort} \sim \text{Condition} + \text{Sex} + (1|\text{Participant}) \quad (1)$$

The linear mixed model provided the effect sizes and uncorrected *P* values for the fixed factors. We corrected the *P* values for multiple comparisons (six tasks) using the Holm-Bonferroni correction. For the postfatigue performance and posture metrics, a similar linear mixed model included additional fixed effects of order (no-exo versus exo condition) and prefatigue workload (number of LL repetitions required to fatigue), without having to correct for multiple comparisons. The workload was log-transformed before analysis and mean-centered for each sex and condition combination.

Supplementary Materials

The PDF file includes:
Methods
Figs. S1 to S10
Tables S1 to S5

Other Supplementary Material for this manuscript includes the following:
MDAR Reproducibility Checklist

REFERENCES AND NOTES

1. National Safety Council, *Fatigue in Safety-Critical Industries: Impact, Risks and Recommendations* (National Safety Council, 2018); www.nsc.org/getmedia/4b5503b3-5e0b-474d-af19-c419cedb4c17/fatigue-in-safety-critical-industries.pdf.aspx.
2. M. Zhang, L. A. Murphy, D. Fang, A. J. Caban-Martinez, Influence of fatigue on construction workers' physical and cognitive function. *Occup. Med.* **65**, 245–250 (2015).
3. R. M. Enoka, J. Duchateau, Translating fatigue to human performance. *Med. Sci. Sports Exerc.* **48**, 2228–2238 (2016).
4. Canadian Centre for Occupational *Health and Safety, Work-Related Musculoskeletal Disorders (WMSDs) - Risk Factors* (Canadian Centre for Occupational Health and Safety, 2019); www.ccohs.ca/oshanswers/diseases/wmsd/risk.pdf.
5. US Bureau of Labor Statistics, "Employer-reported workplace injuries and illnesses – 2021-2022" (Tech. Rep. USDL-22-2139, US Department of Labor, 2021); www.bls.gov/news.release/pdf/osh.pdf.
6. S. D. Wami, G. Abere, A. Dessie, D. Getachew, Work-related risk factors and the prevalence of low back pain among low wage workers: Results from a cross-sectional study. *BMC Public Health* **19**, 1072 (2019).
7. Bone and Joint Initiative USA, *The Hidden Impact of Musculoskeletal Disorders on Americans* (Bone and Joint Initiative USA, ed. 4, 2018); www.boneandjointburden.org/docs/BMUS%20Impact%20of%20MSK%20on%20Americans%20booklet_4th%20Edition%20%282018%29.pdf.
8. D. Wang, F. Dai, X. Ning, Risk assessment of work-related musculoskeletal disorders in construction: State-of-the-art review. *J. Constr. Eng. Manag.* **141**, 04015008 (2015).
9. L. Straker, Evidence to support using squat, semi-squat and stoop techniques to lift low-lying objects. *Int. J. Ind. Ergon.* **31**, 149–160 (2003).
10. E. Welbergen, H. C. Kemper, J. J. Knibbe, H. M. Toussaint, L. Clysen, Efficiency and effectiveness of stoop and squat lifting at different frequencies. *Ergonomics* **34**, 613–624 (1991).
11. K. B. Hagen, K. Harms-Ringdahl, Ratings of perceived thigh and back exertion in forest workers during repetitive lifting using squat and stoop techniques. *Spine* **19**, 2511–2517 (1994).
12. K. B. Hagen, J. Hallen, K. Harms-Ringdahl, Physiological and subjective responses to maximal repetitive lifting employing stoop and squat technique. *Eur. J. Appl. Physiol. Occup. Physiol.* **67**, 291–297 (1993).
13. B. Bazrgari, A. Shirazi-Adl, N. Arjmand, Analysis of squat and stoop dynamic liftings: Muscle forces and internal spinal loads. *Eur. Spine J.* **16**, 687–699 (2007).
14. J. R. Potvin, S. M. McGill, R. W. Norman, Trunk muscle and lumbar ligament contributions to dynamic lifts with varying degrees of trunk flexion. *Spine* **16**, 1099–1107 (1991).
15. D. K. Damkot, M. H. Pope, J. Lord, J. W. Frymoyer, The relationship between work history, work environment and low-back pain in men. *Spine* **9**, 395–399 (1984).
16. L. Straker, P. Duncan, Psychophysical and psychosocial comparison of squat and stoop lifting by young females. *Aust. J. Physiother.* **46**, 27–32 (2000).
17. A. van der Have, S. Van Rossom, I. Jonkers, Squat lifting imposes higher peak joint and muscle loading compared to stoop lifting. *Appl. Sci.* **9**, 3794 (2019).
18. National Institute for Occupational Safety and Health Centers (NIOSH) for Disease Control and Prevention, "Ergonomic guidelines for manual material handling," (Publication 2007-131, California Department of Industrial Relations, 2007); www.cdc.gov/niosh/docs/2007-131/pdfs/2007-131.pdf?id=10.26616/NIOSHPUB2007131.
19. M. Sharp, M. Rosenberger, J. Knapik, "Chapter 5 – Common military task: Materials handling," (Publication RTO-TR-IST-999, Defense Technical Information Center, 2006); https://apps.dtic.mil/sti/pdfs/ADA472464.pdf.
20. US Army Center For Health Promotion And Preventive Medicine, *Lifting Techniques* (US Army Center For Health Promotion and Preventive Medicine, 2000); www.sfdph.org/dph/files/OSH/armylift.pdf.
21. D. Nolan, K. O'Sullivan, J. Stephenson, P. O'Sullivan, M. Lucock, What do physiotherapists and manual handling advisors consider the safest lifting posture, and do back beliefs influence their choice? *Musculoskelet. Sci. Pract.* **33**, 35–40 (2018).
22. I. Ahmad, J.-K. Kim, Assessment of whole body and local muscle fatigue using electromyography and a perceived exertion scale for squat lifting. *Int. J. Environ. Res. Public Health* **15**, 784 (2018).
23. H. Trafimow, O. D. Schipplein, G. J. Novak, G. B. Andersson, The effects of quadriceps fatigue on the technique of lifting. *Spine* **18**, 364–367 (1993).
24. M. Sasaki, A. Horio, M. Wakasa, S. Uemura, Y. Osawa, Influence of quadriceps femoris fatigue on low back load during lifting of loads at different distances from the toes. *J. Phys. Ther. Sci.* **20**, 81–89 (2008).
25. G. M. U. Ghori, R. G. Luckwill, Responses of the lower limb to load carrying in walking man. *Eur. J. Appl. Physiol. Occup. Physiol.* **54**, 145–150 (1985).
26. R. Orr, R. Pope, T. J. A. Lopes, D. Leyk, S. Blacker, B. S. Bustillo-Aguirre, J. J. Knapik, Soldier load carriage, injuries, rehabilitation and physical conditioning: An international approach. *Int. J. Environ. Res. Public Health* **18**, 4010 (2021).
27. M. K. Chung, Y. J. Lee, I. Lee, K. I. Choi, Physiological workload evaluation of carrying soft drink beverage boxes on the back. *Appl. Ergon.* **36**, 569–574 (2005).
28. K. DiVincenzo, Carrying up stairs & keeping your workers safe on the job, *Work Fit* (2018); www.work-fit.com/blog/carrying-up-stairs-keeping-your-workers-safe-on-the-job.
29. H.-C. Chung, M.-J. J. Wang, The effects of container design and stair climbing on maximal acceptable lift weight, wrist posture, psychophysical, and physiological responses in wafer-handling tasks. *Appl. Ergon.* **32**, 593–598 (2001).
30. National Institute for Occupational Safety and Health, *Engineering Controls Database - Material Handling* (National Institute for Occupational Safety and Health, 2018); www.cdc.gov/niosh/engcontrols/ecd/detail25.html.
31. N. J. Givoni, T. Pham, T. J. Allen, U. Proske, The effect of quadriceps muscle fatigue on position matching at the knee. *J. Physiol.* **584**, 111–119 (2007).
32. R. Ranaweera, R. Gopura, T. Jayawardena, G. Mann, Development of a passively powered knee exoskeleton for squat lifting. *J. Robot. Netw. Artif. Life* **5**, 45–51 (2018).
33. R. Hidayah, D. Sui, K. A. Wade, B.-C. Chang, S. Agrawal, Passive knee exoskeletons in functional tasks: Biomechanical effects of a SpringExo coil-spring on squats. *Wearable Technol.* **2**, e7 (2021).
34. T. Bosch, J. van Eck, K. Knitel, M. de Looze, The effects of a passive exoskeleton on muscle activity, discomfort and endurance time in forward bending work. *Appl. Ergon.* **54**, 212–217 (2016).

35. S. J. Baltrusch, J. H. van Dieën, S. M. Bruijn, A. S. Koopman, C. A. M. van Bennekom, H. Houdijk, The effect of a passive trunk exoskeleton on metabolic costs during lifting and walking. *Ergonomics* **62**, 903–916 (2019).
36. M. Goršič, Y. Song, B. Dai, D. Novak, Evaluation of the HeroWear Apex back-assist exosuit during multiple brief tasks. *J. Biomech.* **126**, 110620 (2021).
37. S. Koopman, S. Toxiri, V. Power, I. Kingma, J. H. van Dieën, J. Ortiz, M. P. de Looze, The effect of control strategies for an active back-support exoskeleton on spine loading and kinematics during lifting. *J. Biomech.* **91**, 14–22 (2019).
38. U. Heo, S. J. Kim, J. Kim, Backdrivable and fully-portable pneumatic back support exoskeleton for lifting assistance. *IEEE Robot. Autom. Lett.* **5**, 2047–2053 (2020).
39. T. Poliero, M. Lazzaroni, S. Toxiri, C. Di Natali, D. G. Caldwell, J. Ortiz, Applicability of an active back-support exoskeleton to carrying activities. *Front. Robot. AI* **7**, 579963 (2020).
40. T. Poliero, M. Sposito, S. Toxiri, C. D. Natali, M. Iurato, V. Sanguineti, D. G. Caldwell, J. Ortiz, Versatile and non-versatile occupational back-support exoskeletons: A comparison in laboratory and field studies. *Wearable Technol.* **2**, e12 (2021).
41. F. Sado, H. J. Yap, R. A. R. Ghazilla, N. Ahmad, Design and control of a wearable lower-body exoskeleton for squatting and walking assistance in manual handling works. *Mechatronics* **63**, 102272 (2019).
42. P. Kantharaju, H. Jeong, S. Ramadurai, M. Jacobson, H. Jeong, M. Kim, Reducing squat physical effort using personalized assistance from an ankle exoskeleton. *IEEE Trans. Neural Syst. Rehabil. Eng.* **30**, 1786–1795 (2022).
43. H. Jeong, P. Haghighat, P. Kantharaju, M. Jacobson, H. Jeong, M. Kim, Muscle coordination and recruitment during squat assistance using a robotic ankle–foot exoskeleton. *Sci. Rep.* **13**, 1363 (2023).
44. M.-K. Kim, K.-T. Yoo, The effects of open and closed kinetic chain exercises on the static and dynamic balance of the ankle joints in young healthy women. *J. Phys. Ther. Sci.* **29**, 845–850 (2017).
45. WIRED, Stress testing real-life robot legs | WIRED (2021); www.youtube.com/watch?v=CKvEBWaPd2I.
46. H. Zhu, C. Nesler, N. Divekar, V. Peddinti, R. D. Gregg, Design principles for compact, backdrivable actuation in partial-assist powered knee orthoses. *IEEE/ASME Trans. Mechatron.* **26**, 3104–3115 (2021).
47. B. Laschowski, J. McPhee, Energy-efficient actuator design principles for robotic leg prostheses and exoskeletons: A review of series elasticity and backdrivability. *J. Comput. Nonlinear Dyn.* **18**, 060801 (2023).
48. C. Nesler, G. Thomas, N. Divekar, E. J. Rouse, R. D. Gregg, Enhancing voluntary motion with modular, backdrivable, powered hip and knee orthoses. *IEEE Robot. Autom. Lett.* **7**, 6155–6162 (2022).
49. C. Nuesslein, K. Bhakta, J. Fernandez, F. Davenport, J. Leestma, R. Kim, D. Lee, A. Mazumdar, G. Sawicki, A. Young, Comparing metabolic cost and muscle activation for knee and back exoskeletons in lifting. *IEEE Trans. Med. Robot. Bionics* **6**, 224–234 (2024).
50. A. J. Young, H. Gannon, D. P. Ferris, A biomechanical comparison of proportional electromyography control to biological torque control using a powered hip exoskeleton. *Front. Bioeng. Biotechnol.* **5**, 37 (2017).
51. G. M. Gasparri, J. Luque, Z. F. Lerner, Proportional joint-moment control for instantaneously adaptive ankle exoskeleton assistance. *IEEE Trans. Neural Syst. Rehabil. Eng.* **27**, 751–759 (2019).
52. I. Kang, D. D. Molinaro, G. Choi, J. Camargo, A. J. Young, Subject-independent continuous locomotion mode classification for robotic hip exoskeleton applications. *IEEE Trans. Biomed. Eng.* **69**, 3234–3242 (2022).
53. R. L. Medrano, G. C. Thomas, C. G. Keais, E. J. Rouse, R. D. Gregg, Real-time gait phase and task estimation for controlling a powered ankle exoskeleton on extremely uneven terrain. *IEEE Trans. Robot.* **39**, 2170–2182 (2023).
54. D. D. Molinaro, I. Kang, A. J. Young, Estimating human joint moments unifies exoskeleton control, reducing user effort. *Sci. Robot.* **9**, eadi8852 (2024).
55. P. Slade, M. J. Kochenderfer, S. L. Delp, S. H. Collins, Personalizing exoskeleton assistance while walking in the real world. *Nature* **610**, 277–282 (2022).
56. I. Lin, N. Divekar, G. Lv, R. D. Gregg, Energy shaping control with virtual spring and damper for powered exoskeletons, in *2019 IEEE 58th Conference on Decision and Control (CDC)* (IEEE, 2019), pp. 3039–3045.
57. I. Lin, N. V. Divekar, G. C. Thomas, R. D. Gregg, Optimally biomimetic passivity-based control of a lower-limb exoskeleton over the primary activities of daily life. *IEEE Open J. Control Syst.* **1**, 15–28 (2022).
58. T. Luger, M. Bär, R. Seibt, M. A. Rieger, B. Steinhilber, Using a back exoskeleton during industrial and functional tasks—effects on muscle activity, posture, performance, usability, and wearer discomfort in a laboratory trial. *Hum. Factors* **65**, 5–21 (2023).
59. T. D. O'Brien, N. D. Reeves, V. Baltzopoulos, D. A. Jones, C. N. Maganaris, In vivo measurements of muscle specific tension in adults and children. *Exp. Physiol.* **95**, 202–210 (2010).
60. N. V. Divekar, J. Lin, C. Nesler, S. Borboa, R. D. Gregg, A potential energy shaping controller with ground reaction force feedback for a multi-activity knee-ankle exoskeleton, in *2020 8th IEEE RAS/EMBS International Conference for Biomedical Robotics and Biomechatronics (BioRob)* (IEEE, 2020), pp. 997–1003.
61. I. Demers, R. Weiss-Lambrou, B. Ska, The Quebec User Evaluation of Satisfaction with Assistive Technology (QUEST 2.0): An overview and recent progress. *Technol. Disabil.* **14**, 101–105 (2002).
62. I. Camargo, A. Ramanathan, W. Flanagan, A. Young, A comprehensive, open-source dataset of lower limb biomechanics in multiple conditions of stairs, ramps, and level-ground ambulation and transitions. *J. Biomech.* **119**, 110320 (2021).
63. J. Grimmer, J. Zeiss, F. Weigand, G. Zhao, S. Lamm, M. Steil, A. Heller, Lower limb joint biomechanics-based identification of gait transitions in between level walking and stair ambulation. *PLOS ONE* **15**, e0239148 (2020).
64. E. Reznick, K. R. Embry, R. Neuman, E. Bolívar-Nieto, N. P. Fey, R. D. Gregg, Lower-limb kinematics and kinetics during continuously varying human locomotion. *Sci. Data* **8**, 282 (2021).
65. C.-K. Chan, H. N. Azah, C.-H. Yeow, S.-K. Goh, H.-N. Ting, K. Salmah, Effects of squatting speed and depth on lower extremity kinematics, kinetics and energetics. *J. Mech. Med. Biol.* **22**, 2250032 (2022).
66. A. Arefeen, Y. Xiang, Subject specific optimal control of powered knee exoskeleton to assist human lifting tasks under controlled environment. *Robotica* **41**, 2809–2828 (2023).
67. H. S. Longpré, S. M. Acker, M. R. Maly, Muscle activation and knee biomechanics during squatting and lunging after lower extremity fatigue in healthy young women. *J. Electromyogr. Kinesiol.* **25**, 40–46 (2015).
68. D. Staudenmann, K. Roeleveld, D. F. Stegeman, J. H. van Dieën, Methodological aspects of SEMG recordings for force estimation—A tutorial and review. *J. Electromyogr. Kinesiol.* **20**, 375–387 (2010).
69. I. T. Picchiotti, E. B. Weston, G. G. Knapik, J. S. Dufour, W. S. Marras, Impact of two postural assist exoskeletons on biomechanical loading of the lumbar spine. *Appl. Ergon.* **75**, 1–7 (2019).
70. J. Kompf, O. Arandjelovic, Understanding and overcoming the sticking point in resistance exercise. *Sports Med.* **46**, 751–762 (2016).
71. National Register of Personal Trainers, "Squats test"; https://nrpt.co.uk/training/tests/strength/squats.htm.
72. E. P. Lamers, J. C. Soltys, K. L. Scherpereel, A. J. Yang, K. E. Zelik, Low-profile elastic exosuit reduces back muscle fatigue. *Sci. Rep.* **10**, 15958 (2020).
73. G. Lv, H. Zhu, R. D. Gregg, On the design and control of highly backdrivable lower-limb exoskeletons: A discussion of past and ongoing work. *IEEE Control Syst. Mag.* **38**, 88–113 (2018).
74. J. Lin, N. V. Divekar, G. Lv, R. D. Gregg, Optimal task-invariant energetic control for a knee-ankle exoskeleton. *IEEE Control Syst. Lett.* **5**, 1711–1716 (2021).
75. D. J. Villarreal, R. D. Gregg, A survey of phase variable candidates of human locomotion, in *2014 36th Annual International Conference of the IEEE Engineering in Medicine and Biology Society* (IEEE, 2014), pp. 4017–4021.
76. S. Zhao, K. Walters, J. M. Perez, R. D. Gregg, Design and validation of a modular, backdrivable ankle exoskeleton, paper presented at IEEE International Conference on Biomedical Robotics and Biomechatronics, 1 to 4 September 2024, Heidelberg, Germany; https://locolab.robotics.umich.edu/documents/ZhaoWaltersGregg-BioRob2024.pdf.
77. J. Lin, G. C. Thomas, N. V. Divekar, V. Peddinti, R. D. Gregg, A modular framework for task-agnostic, energy shaping control of lower limb exoskeletons. *IEEE Trans. Control Syst. Technol.* 10.1109/TCST.2024.3429908 (2024).
78. Vicon Motion Systems, *Upper Body Modeling with Plug-in Gait - Nexus 2.13 Documentation - Vicon Documentation* (Vicon Motion Systems, 2023); https://help.vicon.com/space/Nexus216/11602259/Upper+body+modeling+with+Plug-in+Gait.
79. Vicon Motion Systems, *BodyBuilder for Biomechanics* (Vicon Motion Systems, 1997); https://www.vicon.com/software/bodybuilder/.

Acknowledgments: We thank J. Lin for controls consultations, V. Peddinti for electronics consultations, C. Powell for statistical consultations, D. Prins for sports science consultations, E. Rouse and C. Krishnan for data analysis consultations, J. Zhang for help during experiments, P. Divekar for illustrations, and K. Best for general help. **Funding:** This work was supported by the National Institutes of Health (grant R01EB031166 to R.D.G.).
Author contributions: Conceptualization: N.V.D. and R.D.G. Data curation: N.V.D. Formal analysis: N.V.D. and A.R.Y. Funding acquisition: R.D.G. Investigation: N.V.D. and H.B.F. Methodology: N.V.D., G.C.T., H.B.F., and R.D.G. Project administration: H.B.F. and R.D.G. Software: N.V.D., G.C.T., and A.R.Y. Supervision: R.D.G. Visualization: N.V.D. Writing—original draft: N.V.D., A.R.Y., and R.D.G. Writing—review and editing: N.V.D. and R.D.G.
Competing interests: R.D.G. and N.V.D. are authors of the provisional patent application titled "Limb-assistive device with modified energy shaping," with US Patent serial no. 63/663,493. The other authors declare that they have no competing interests. **Data and materials availability:** The paper, its Supplementary Materials, and the Dryad dataset (DOI: 10.5061/dryad.z34tmpgks) contain all of the necessary data to assess the

conclusions. Dryad contains data files S1 and S2. Data file S1: Session 1—for each participant and condition: normalized EMG profiles and mean values for each LLC task; exoskeleton torque, GRF, sagittal knee angle, sagittal thigh angle, and sagittal shank angle profiles for each LLC task. Data file S2: Session 2—for each participant and condition: repetition duration, thorax lean (raw and deviation), and peak knee angle (raw and deviation) across LL trial progression; 10 postfatigue squat LL repetition completion time deficit; mean thorax lean (raw and deviation), and mean peak knee angle (raw and deviation) of 10 postfatigue squat LL repetitions; and postfatigue modified QUEST feedback ratings for each LLC task.

Submitted 17 July 2024
Accepted 23 August 2024
Published 18 September 2024
10.1126/scirobotics.adr8282

Science Robotics

A versatile knee exoskeleton mitigates quadriceps fatigue in lifting, lowering, and carrying tasks

Nikhil V. Divekar, Gray C. Thomas, Avani R. Yerva, Hannah B. Frame, and Robert D. Gregg

Sci. Robot. **9** (94), eadr8282. DOI: 10.1126/scirobotics.adr8282

Editor's summary
Fatigue among workers engaging in physically demanding tasks increases their risk of injury. In particular, fatigue-induced musculoskeletal injuries occur because of repeated lifting, lowering, and carrying activities among workers. Divekar *et al*. have developed an adaptive knee exoskeleton controller that provides assistance to users depending on the tasks carried out. The exoskeleton controller was capable of application-specific tuning without user calibration. It was shown to minimize quadriceps muscle fatigue among participants carrying out repetitive multiterrain lifting, lowering, and carrying tasks. —Amos Matsiko

Science Robotics (ISSN 2470-9476) is published by the American Association for the Advancement of Science. 1200 New York Avenue NW, Washington, DC 20005. The title *Science Robotics* is a registered trademark of AAAS.